Al3 positions deviate considerably from full occupancy, with the occupation factors 0.36 and 0.23, respectively. Remarkable anisotropy of thermal motion of Al2 and Al3 atoms ($B33$ is larger than $B11$ and $B22$) correlates with the electron-density distribution in the (100) plane (see Fig. 2). The Fe and Al1 atoms are placed in the same positions, as in the former approximate structure proposal.

The partial occupation of aluminium positions Al2 and Al3 in the Fe_2Al_5 structure leads to a different atomic coordination compared with the former proposal (Fig. 3). Some edges of coordination polyhedra became more diffuse with respect to the non-ordered location of atoms on them. The coordination polyhedron of the Fe atom has one such edge, the coordination polyhedron of the Al1 atom has two. The coordination figures of Al2 and Al3 atoms are comparable with the coordination polyhedron of the Al2 atom in the former model, if the overlapping atoms were excluded from the coordination sphere.

One of the possible reasons for the non-ordered distribution of Al atoms along the [001] axis could arise from interactions of Fe and Al1 atoms, which build the three-dimensional framework with the channels located along the [001] axis (Fig. 4). The interatomic distances between atoms building this framework are from 2.5 to 2.66 Å and are *ca* 8% shorter than the sum of atomic radii ($r_{Fe} + r_{Al}$ = 2.69 Å, $2r_{Al}$ = 2.86 Å). The channels have the shape of pentagonal antiprisms and are connected by side edges. There are two types of points on the axes of the channels; atoms on these points presumably have more stronger interactions with the Fe atoms from the framework (the respective distances between the Fe atoms and these points are *ca* 2.36 Å). In fact, both positions are occupied by the Al atoms (Al2 and Al3). As the positions are very close to each other (see Table 2), both of them cannot be occupied at the same time and consequently the occupation of these sites is incomplete.

This investigation was supported by the Deutsche Forschungsgemeinschaft.

References

AKSELRUD, L. G., GRIN, YU. N., ZAVALII, P. YU., PECHARSKY, V. K. & FUNDAMENSKI, V. S. (1989). *Collected Abstracts of 12th European Crystallography Meeting*, Vol. 3, p. 155. Moscow: Academy of Sciences of the USSR.

ELLNER, M. & MAYER, J. (1992). *Scr. Metall.* **26**, 501-504.

GRIGER, A., STEFANIAY, V. & TURMEZEY, T. (1986). *Z. Metallkd.* **77**, 30-35.

HAMILTON, W. (1965). *Acta Cryst.* **18**, 502-510.

MARTON, L. (1959). *Methods of Experimental Physics*, Vol. 1, p. 68. New York: Academic Press.

MASSALSKI, T. B., OKAMOTO, H., SUBRAMANIAN, P. R. & KACPRZAK, L. (1990). *Binary Alloy Phase Diagrams*, 2nd ed., Vol. 1, pp. 147-149. Materials Park, OH: ASM International.

SCHÜBERT, K. (1964). *Kristallstrukturen Zweikomponentiger Phasen*, pp. 295-297. Berlin: Springer-Verlag.

SCHUBERT, K. & KLUGE, M. (1953). *Z. Naturforsch. Teil A*, **8**, 755-756.

SCHUBERT, K., RÖSLER, U., KLUGE, M., ANDERKO, K. & HÄRLE, L. (1953). *Naturwissenschaften*, **40**, 437.

Acta Cryst. (1994). **B50**, 316–326

The Synergetic Effect in Beryllium Sulfate Tetrahydrate – an Experimental Electron-Density Study*

BY THOMAS KELLERSOHN†

Anorganische Chemie I, *Universität GH Siegen, Postfach* 101240, *D*-57068 *Siegen, Germany*

AND ROBERT G. DELAPLANE AND IVAR OLOVSSON‡

Department of Inorganic Chemistry, Institute of Chemistry, Uppsala University, Box 531, *S*-751 21 *Uppsala, Sweden*

(*Received* 16 *March* 1993; *accepted* 10 *January* 1994)

Dedicated to Professor H. D. Lutz on the occasion of his 60*th birthday*

Abstract

The electron density in piezoelectric beryllium sulfate tetrahydrate has been determined by multipole refinement of single-crystal X-ray data collected at 30 K. Hydrogen positional and displacement parameters have been taken from a refinement using single-crystal neutron data. Structural parameters are also given based on single-crystal neutron data collected at 100 and 295 K. The Be^{2+} ion causes a strong polarization of the lone-pair density of the water O atom. Only a single maximum of the deformation density is observed in this region. The polarization is

* Hydrogen Bond Studies. 158. Part 157: Kellersohn, Delaplane, Olovsson & McIntyre (1993).

† Present address: Editorial Department, VCH Publishers, Postfach 101161, D-69451 Weinheim, Germany.

‡ To whom correspondence should be addressed.

transferred to the hydrogen bonds which are, therefore, stronger than in most other sulfate hydrates. This so-called 'synergetic effect' is evidenced from the charge depletion close to the hydrogen nuclei, the very short hydrogen-bond distances as well as from the low OH stretching frequencies. Therefore, the present study reveals clearly the interplay between geometric, electronic and energetic factors which influence hydrogen bonds in solids. Additionally, the deformation density of the water molecule compares well with the results of *ab initio* calculations. It is found that superposition effects on the individual deformation densities can be reduced when the γ parameters, which govern the breadth of the radial functions, are modified to 'chemically reasonable' values. Crystal data: $BeSO_4.4H_2O$, $M_r = 177.14$, tetragonal, $I\bar{4}c2$, $Z = 4$; λ(Mo $K\alpha$) = 0.71073 Å, μ = 4.456 cm^{-1}, $F(000) = 368$. $T1 = 30$ K: $a = 8.0120$ (5), $c = 10.712$ (1) Å, $V = 687.6$ (1) Å^3, D_x = 1.711 Mg m^{-3}, $R(F) = 0.0124$ for 1742 reflections (X-ray); $\lambda = 1.037$ Å, $\mu = 1.71$ cm^{-1}, $F(000)$ = 108.60 fm, $R(F) = 0.0243$ for 540 reflections (neutron). $T2 = 100$ K: $a = 7.9986$ (6), c = 10.705 (1) Å, $V = 684.9$ (1) Å^3, $D_x = 1.718$ Mg m^{-3}, $R(F) = 0.0249$ for 543 reflections (neutron). $T3$ = 295 K: $a = 7.9922$ (9), $c = 10.702$ (2) Å, V = 683.6 (1) Å^3, $D_x = 1.721$ Mg m^{-3}, $R(F) = 0.0287$ for 411 reflections (neutron).

1. Introduction

The seemingly surprising situation that many relatively simple beryllium compounds are not well characterized might be due to the great latent toxicity which beryllium ions exhibit to biological systems. This alone calls for more detailed investigations. Since water is *the* ubiquitary solvent, it is interesting to explore the Be^{2+}–H_2O interaction in the $[Be(H_2O)_4]^{2+}$ complex cation by a careful electron-density analysis. Few investigations of this kind have hitherto been performed on beryllium compounds.

Beryllium sulfate tetrahydrate is somewhat exceptional, since it has been studied by several methods in the past. Its crystal structure has been determined by Beevers & Lipson (1932) and refined by Dance & Freeman (1969) from single-crystal X-ray photographic data. Independently, a neutron diffraction study was performed by Sikka & Chidambaram (1969). All these investigations were performed at room temperature. Vibrational spectroscopic studies have been performed by Soulmagnon & Couture-Mathieu (1950), Katiyar & Krishnamurthy (1969), Unger (1972), Srivastava, Khandelwal & Bist (1976*a*,*b*) and Pigenet (1982*a*,*b*). The goal in solid-state nuclear magnetic resonance studies on $BeSO_4.4D_2O$ (Berglund & Tegenfeldt, 1977) was to determine the electric field gradient tensors at the deuteron sites, whereas further investigations by the same method and by *ab initio* calculations (Larsson & Tegenfeldt, 1988; Larsson, Tegenfeldt & Hermansson, 1991) were performed to investigate the activation barrier for the 180° flip motion of the water molecules around the axis bisecting the HOH angle.

These previous studies provide the background for an electron-density study. We chose $BeSO_4.4H_2O$ as a model system for additional reasons. The good availability and stability facilitate the handling of the samples; large good quality crystals for the neutron diffraction studies can quite easily be grown. The atoms are light (even the somewhat heavier sulfur was not expected to be a severe limitation). The structure is relatively simple with high symmetry, reducing the number of refineable parameters and unique reflections. This is helpful for obtaining statistically meaningful standard deviations for I(obs) by merging symmetry-related reflections, whereas the limited number of independent reflections to be measured facilitates studies at different temperatures.

Our interest focuses on the water molecules and the hydrogen bonds, which provide the chemical motivation for this work. The hydrogen bonds in $BeSO_4.4H_2O$ are among the strongest donated by water molecules in solid hydrates, as shown by both the short O···O and H···O distances and the low frequencies of the OH stretching vibrations (for a review see Lutz, 1988). The water O atoms have almost ideal trigonal coordination (class 1 according to Chiari & Ferraris, 1982), which usually occurs in the presence of highly charged small cations. However, such cations are commonly heavier, having considerably more core electrons than Be^{2+}, which is the only example from the first period. There have been some theoretical calculations on the electron redistribution of trigonally coordinated water molecules (see, for example, Hermansson, Olovsson & Lunell, 1984; Hermansson, 1985), but an experimental study for a directly comparable configuration has so far been missing.

It should be noted that earlier electron-density studies on transition-metal salt hydrates containing more or less perfectly trigonally coordinated water molecules focus on the *d*-electron redistribution around the metal ions and little attention was paid to features around the water molecules. This is not too surprising, since dominant scatterers frequently prevent a conclusive interpretation of comparatively small features. However, a multipole refinement procedure with chemical restraints, separating the contributions of the various constituents of the crystal, makes it possible to extract information of this type (McIntyre, Ptasiewicz-Bak & Olovsson, 1990;

Table 1. *Data collection and refinement parameters for* $BeSO_4.4H_2O$

Abbreviations: conv. = conventional refinement, h.-a. = high-angle refinement, def. = deformation refinement. More crystal data are given in the *Abstract*.

	Neutron			X-ray				
	30 K	100 K	300 K	30 K			100 K	300 K
No. of measured reflections	769	765	629	3416			2193	5216
2θ range	3–107	3–107	3–100	2–110			2–110	2–85
$[(\sin\theta)/\lambda]_{max}$ (Å^{-1})	0.775	0.775	0.739	1.153			1.153	0.951
Min./max. h	−12/0	−12/0	−11/0	−17/17			−17/17	−15/15
Min./max. k	−12/0	−12/0	−11/0	−17/17			−17/17	−15/15
Min./max. l	0/16	0/16	0/14	−22/22			0/22	−20/20
R_{int} (I)	—	—	—	0.0257			0.0207	0.0318
Total measuring time (h)	84	84	75	218			138	327
Decay correction (%)	−0.7	−1.3	−0.1	−3.0			−0.2	−2.2
Type of refinement	conv.	conv.	conv.	conv.	h.-a.	def.	conv.	conv.
Cutoff, $I > x\sigma(I)$; x =	3.0	3.0	3.0	3.0	3.0	0	3.0	3.0
Reflections used	540	543	411	1697	612	1742	1693	1014
No. of parameters	47	47	47	24	23	117	24	24
k in weighting scheme	0.037	0.035	0.045	0.040	0.035	0.022	0.040	0.050
$[(\sin\theta)/\lambda]_{min}$ (Å^{-1})	0.0	0.0	0.0	0.0	0.90	0.0	0.0	0.0
$R(F^2)$	0.0332	0.0349	0.0425	0.0409	0.0308	0.0197	0.0465	0.0511
$wR(F^2)$	0.0430	0.0449	0.0574	0.0542	0.0471	0.0309	0.0597	0.0727
$R(F)$	0.0243	0.0249	0.0287	0.0191	0.0186	0.0124	0.0235	0.0286
S	1.032	1.120	1.095	1.132	0.890	1.012	1.120	1.092
δR plot: slope	1.01	0.94	1.04	0.95	1.14	1.02	0.92	0.97
y intercept	−0.06	−0.06	−0.02	−0.05	−0.02	−0.02	−0.06	−0.09
Reflections with $\lvert\Delta\rvert > 4\sigma$	0	1	1	14	0	0	9	4

Olovsson, Ptasiewicz-Bak & McIntyre, 1993; Kellersohn, Delaplane, Olovsson & McIntyre, 1993). In contrast to the restrictions in the previous studies, the present investigation attempts to model the deformation density of the bound water molecules with a highly flexible set of deformation functions. Preliminary results have been reported (Kellersohn, Delaplane & Olovsson, 1991).

2. Experimental

Slow evaporation at 295 K of a concentrated solution of $BeSO_4.4H_2O$ in dilute sulfuric acid produced colourless single crystals. The data-collection parameters for the X-ray and neutron experiments are listed in Table 1; further information is given below.

Neutron data

The positional and thermal parameters of the H atoms used in deformation analyses are usually taken from a neutron diffraction experiment. Since the previous study (Sikka & Chidambaram, 1969) was performed at room temperature and no absorption correction was applied, we collected new data at 30, 100 and 295 K.

The crystal for these data collections was a truncated octahedron which exhibited solely {112} forms with maximum dimensions 5.6, 2.8 and 4.1 mm, and calculated volume 60.5 mm^3. Reflection intensities were measured on a Huber–Aracor four-circle diffractometer equipped with a 400 mm χ-circle and a two-stage closed-cycle helium refrigerator (Samson, Goldish & Dick, 1980) at the R2 reactor at Studsvik, Sweden, with the beam wavelength 1.037 Å determined by reflection from a Cu (220) double monochromator. Data collection in the ω–2θ mode, step scans, $\Delta\omega = 0.010$ with a minimum of 70 steps, maximum measuring time 3 s step^{-1}. The temperature stability of ±0.5 K with an absolute inaccuracy of ±2 K was estimated from previous calibrations against the transition temperatures of KDP (122 K) and $KMnF_3$ (81 K).

Cell dimensions determined from the orientation matrices agreed well with the X-ray values in each case. Background corrections according to Lehmann & Larsen (1974) and Lorentz corrections were applied; an absorption correction was applied to each data set by Gaussian integration using an experimentally determined absorption coefficient $\mu = 1.71$ cm^{-1}, transmission range 0.500–0.670.

X-ray data

A rectangular prismatic crystal was used with boundary planes (100), ($\bar{1}$00), (010), (0$\bar{1}$0), (001) and (00$\bar{1}$); size 0.228 × 0.183 × 0.151 mm; volume 6.3×10^{-3} mm^3. The intensity measurement was performed on a Huber–Aracor four-circle diffractometer analogous to the neutron data collection. Graphite (002) monochromatized Mo $K\alpha$ radiation was used. Cell dimensions were determined by a least-squares fit of setting angles for 34 well centred reflections in the range $25 < \theta < 30$°. A linear decay correction was applied, absorption correction by

Table 2. *Refined positional and anisotropic displacement parameters*

At 30 K. First row: neutron data; second row: conventional refinement; third row: high-angle refinement; fourth row: deformation refinement. Hydrogen positional and displacement parameters were fixed at neutron values for all X-ray refinements.

	x	y	z	U_{11}	U_{22}	U_{33}	U_{12}	U_{13}	U_{23}
30 K data									
Be	0	1/2	1/4	0.151 (12)	U_{11}	0.052 (9)	0	0	0
	0	1/2	1/4	0.181 (5)	U_{11}	0.118 (4)	0	0	0
	0	1/2	1/4	0.205 (7)	U_{11}	0.130 (5)	0	0	0
	0	1/2	1/4	0.189 (4)	U_{11}	0.124 (3)	0	0	0
S	0	0	0	0.111 (25)	U_{11}	0.059 (22)	0	0	0
	0	0	0	0.112 (1)	U_{11}	0.081 (1)	0	0	0
	0	0	0	0.135 (4)	U_{11}	0.097 (2)	0	0	0
	0	0	0	0.125 (1)	U_{11}	0.088 (1)	0	0	0
O(1)	0.12605 (13)	0.08463 (13)	0.07820 (10)	0.199 (15)	0.116 (14)	0.108 (8)	0.041 (10)	−0.049 (8)	−0.035 (8)
	0.12630 (3)	0.08489 (3)	0.07816 (3)	0.241 (2)	0.180 (2)	0.175 (2)	0.012 (2)	−0.094 (2)	−0.051 (1)
	0.12609 (5)	0.08485 (5)	0.07806 (4)	0.267 (5)	0.202 (5)	0.192 (3)	0.014 (2)	−0.093 (2)	−0.050 (2)
	0.12619 (3)	0.08490 (3)	0.07809 (2)	0.253 (2)	0.193 (2)	0.182 (1)	0.013 (2)	−0.094 (1)	−0.051 (1)
O(2)	0.13670 (14)	0.39564 (12)	0.17151 (10)	0.206 (15)	0.186 (15)	0.130 (9)	−0.007 (12)	0.136 (8)	−0.049 (10)
	0.13710 (3)	0.39603 (3)	0.17146 (3)	0.271 (3)	0.188 (2)	0.206 (2)	−0.047 (2)	0.107 (2)	−0.056 (2)
	0.13715 (5)	0.39601 (5)	0.17140 (4)	0.291 (5)	0.217 (5)	0.218 (3)	−0.040 (2)	−0.103 (2)	−0.055 (2)
	0.13714 (3)	0.39602 (3)	0.17138 (3)	0.280 (2)	0.202 (2)	0.210 (1)	−0.043 (2)	0.105 (1)	−0.058 (1)
H(1)	0.23027 (27)	0.45874 (25)	0.13166 (20)	0.541 (28)	0.509 (28)	0.384 (16)	−0.102 (19)	0.194 (19)	0.010 (20)
H(2)	0.12564 (27)	0.28306 (26)	0.13589 (22)	0.645 (29)	0.419 (30)	0.388 (19)	0.006 (19)	0.096 (20)	−0.144 (19)
100 K neutron data									
Be	0	1/2	1/4	0.146 (10)	U_{11}	0.091 (8)	0	0	0
S	0	0	0	0.052 (25)	U_{11}	0.120 (18)	0	0	0
O(1)	0.12615 (16)	0.08475 (15)	0.07798 (13)	0.303 (18)	0.174 (16)	0.222 (9)	0.075 (12)	−0.129 (10)	−0.074 (10)
O(2)	0.13681 (17)	0.39589 (14)	0.17158 (12)	0.327 (18)	0.199 (16)	0.246 (11)	−0.065 (13)	0.225 (10)	−0.087 (11)
H(1)	0.23014 (31)	0.45833 (30)	0.13175 (21)	0.592 (34)	0.585 (33)	0.0436 (18)	−0.115 (24)	0.277 (22)	−0.040 (23)
H(2)	0.12594 (33)	0.28386 (31)	0.13636 (25)	0.745 (35)	0.441 (35)	0.455 (22)	−0.025 (23)	0.140 (24)	−0.131 (21)
300 K neutron data									
Be	0	1/2	1/4	0.499 (16)	U_{11}	0.274 (15)	0	0	0
S	0	0	0	0.399 (31)	U_{11}	0.370 (22)	0	0	0
O(1)	0.12589 (26)	0.08466 (26)	0.07728 (24)	0.922 (35)	0.630 (31)	0.657 (22)	0.152 (21)	−0.299 (20)	−0.246 (19)
O(2)	0.13680 (28)	0.39633 (26)	0.17176 (21)	0.994 (34)	0.603 (31)	0.718 (27)	−0.169 (23)	0.571 (21)	−0.216 (19)
H(1)	0.23046 (46)	0.45847 (51)	0.13168 (40)	1.093 (61)	1.062 (62)	0.786 (41)	−0.162 (40)	0.411 (41)	−0.140 (38)
H(2)	0.12585 (50)	0.28479 (48)	0.13667 (39)	1.324 (64)	0.817 (63)	0.730 (37)	−0.037 (36)	0.185 (45)	−0.112 (40)

Gaussian integration, transmission range 0.908–0.961.

Additionally, the lattice constants were refined and X-ray data sets were collected at 100 and 295 K. The results of these experiments have been deposited.*

3. Refinements

All data-reduction programs and the full-matrix least-squares program *DUPALS* used for the refinements have been described by Lundgren (1982). The atomic positions reported by Sikka & Chidambaram (1969) were taken as starting values in each case. Final agreement indices *etc.* are given in Table 1, atomic coordinates and anisotopic displacement parameters in Table 2.*

* Structural parameters from the conventional and high-angle refinement of the 30 K data, the results of the refinements of the 100 and 295 K neutron and X-ray data as well as tables of observed and calculated structure factors have been deposited with the British Library Document Supply Centre as Supplementary Publication No. SUP 71775 (37 pp.). Copies may be obtained through The Technical Editor, International Union of Crystallography, 5 Abbey Square, Chester CH1 2HU, England. [CIF reference: AB0310]

Neutron data

The scattering lengths used were 7.790, 2.847, 5.803 and −3.739 fm for Be, S, O and H, respectively (Sears, 1986). Due to the perfection and large size of the crystal, a number of reflections were severely affected by extinction. Several extinction models, isotropic as well as anisotropic, within the Becker & Coppens (1974*a*,*b*, 1975) formalism were tried. The best agreement was found for an anisotropic type I model with a Lorentzian anisotropic mosaic-spread distribution, described according to Thornley & Nelmes (1974). The quantity minimized was $\sum w(|F_o| - |F_c|)^2$, where $w^{-1} = \sigma^2_{\text{count}}|F_o| + k^2|F_o|^2$. The constant k was determined empirically from weighting analyses for different values of k. Only those reflections suffering less than 50% from extinction were used in the final refinements. The 47 variable parameters were a scale factor, six anisotropic extinction parameters, and the positional and anisotropic displacement parameters of all atoms.

X-ray data

The quantity minimized was $\sum w(|F_o|^2 - |F_c|^2)^2$, where $w^{-1} = \sigma^2_{\text{count}}|F_o|^2 + k^2|F_o|^4$.

(*a*) *Conventional refinement.* The scale factor, an isotropic extinction parameter (type I, Lorentzian mosiac spread), positional parameters for O atoms and anisotropic displacement parameters for Be, S, and O atoms were refined. The H-atom positional and displacement parameters were taken from the neutron data without modification, although it was noticed that the O-atom displacement parameters for the X-ray and neutron data differed. No clear trend could be established due to the limited number of comparable values. Refinements for the inverse enantiomorph yielded slightly worse R values; therefore, Friedel pairs were not merged.

(*b*) *High-order refinement.* This was based on the reflections having $(\sin\theta)/\lambda > 0.90$ Å^{-1}. The refined parameters were as for the conventional refinements except for the extinction parameter, which was fixed at the previously determined value. The O-atom coordinates agree with the neutron values, but all displacement parameters are closer to the conventional X-ray values than to the neutron values.

(*c*) *Deformation refinements.* To minimize the effects of experimental noise and to reduce the effects of phase errors on X–$X_{\text{high-order}}$ or X–N Fourier syntheses for a non-centrosymmetric structure, electron deformation density modelling by multipole fitting is preferred. We employed the multipole deformation functions proposed by Hirshfeld (1971) with modifications by Harel & Hirshfeld (1975) and Hirshfeld (1977). The spherical charge density at each atomic site is modified by an expansion of up to 35 terms with the general form

$$\rho_n(r,\theta_k) = N_n r^n \exp(-\gamma r^2) \cos^n\theta_k$$

centred on the site, where r and θ_k are polar coordinates in the kth of a chosen set of axes, n and k are integers [$n = 0, 1, 2, 3, 4$; $k = 1, \ldots, (n+1)(n+2)/2$] and N_n are normalization factors. The scattering factor for each atom is then

$$f_i = f_{\text{spher},i} + \sum C_i \varphi_i,$$

where φ_i are the Fourier transforms of the expansion of the deformation density. The (population) parameters C_i are refineable.

A series of deformation refinements was performed, where initially imposed symmetry constraints on the water molecules were progressively relaxed and the value of n increased. The significance of each increase in sophistication of the model was checked by inspecting the goodness-of-fit and the δR plot (Abrahams & Keve, 1971). Through these series the δR plots changed drastically from sigmoidal to a nearly linear shape, which is a good indicator of increasing accuracy for the model. The decreasing wR values and the vanishing number of 'bad' reflections support this. Strong correlation effects prohibited the simultaneous refinement of the γ parameters, which govern the breadth of the radial functions, with the other deformation parameters. Initially these were fixed at 3.5 for each atom, from experience on $NiSO_4.6H_2O$ (McIntyre, Ptasiewicz-Bak & Olovsson, 1990). A subsequent analysis of the present results showed that these values have to be modified to yield chemically reasonable individual deformation-density maps as discussed below.

Only for the 30 K data was it possible to extend the deformation model to the highest level of flexibility, *i.e.* imposing no symmetry constraints on the O atoms and including deformation functions up to the hexadecapole level. In the final set, the following parameters were refined:

Be: $n \le 3$, site symmetry 4, $\gamma = 5.0$, β_{ii} and five deformation parameters.

S: $n \le 4$, site symmetry 4, $\gamma = 2.5$, β_{ii} and 10 deformation parameters.

O: $n \le 4$, no symmetry restrictions, $\gamma = 3.5$, x, y, z, β_{ij} and 35 deformation parameters.

H: $n \le 2$, cylindrical symmetry, $\gamma = 4.0$, x, y, z, β_{ij} fixed to neutron values, five deformation parameters; and additionally, a scale factor and isotropic extinction parameter as in the conventional refinements.

For the 100 and 295 K data, a corresponding set-up produced unacceptable parameter correlations (some larger than 0.95) and distorted maps. However, a restrained deformation refinement using the 100 K data produced sensible maps which did not show global discrepancies compared with the 30 K maps, but with some loss of detail, which could only partly be attributed to thermal smearing. For the 295 K data, the deformation refinement was abandoned due to these difficulties. In the following discussion, only the 30 K results will be considered.*

4. Results and discussion

General features of the structure are described in earlier reports (Dance & Freeman, 1969; Sikka & Chidambaram, 1969). A projection showing the hydrogen-bond connections between the $[Be(H_2O)_4]^{2+}$ and the SO_4^{2-} tetrahedra is given in Fig. 1. The water molecules are bonded to one beryllium ion with the Be—O bond axis deviating by 16.65 (4), 16.49 (4) and 16.59 (4)° (30, 100 and 295 K) from the HOH plane. The deviation from an ideal trigonal planar coordination (where the metal ion is situated on the bisector of the HOH angle) is relatively small. Bond distances and angles are given in Table 3, including values for the water molecules and hydrogen bonds more precise than those reported earlier.

* See deposition footnote.

Table 3. *Interatomic distances* (Å) *and angles* (°) *for* $BeSO_4.4H_2O$ *based on the neutron diffraction data*

Distances corrected for thermal motion (riding model) are given in square brackets.

		30 K		100 K		300 K	
Be coordination							
Be—O(1)	(4×)	1.614 (1)		1.611 (1)		1.607 (2)	
O(1)—Be—O(1)	(2×)	117.22 (7)		117.19 (6)		117.20 (16)	
O(1)—Be—O(1)	(4×)	105.74 (3)		105.75 (4)		105.75 (7)	
Sulfate							
S—O(2)	(4×)	1.477 (1)		1.475 (1)		1.468 (2)	
O(2)—S—O(2)	(2×)	110.89 (8)		111.0 (1)		11.4 (2)	
O(2)—S—O(2)	(4×)	108.76 (4)		108.69 (5)		108.54 (9)	
Water molecules and hydrogen bonds							
O(1)—H(1)		1.000 (2)	[1.015]	0.994 (3)	[1.007]	0.996 (4)	[1.002]
O(1)—H(2)		0.983 (2)	[0.990]	0.976 (3)	[0.980]	0.971 (4)	[0.976]
H(1)—O(1)—H(2)		111.4 (2)		111.2 (2)		111.0 (4)	
H(1)···O(2)		1.634 (2)		1.636 (3)		1.635 (4)	
O(1)—H(1)···O(2)		171.8 (2)		171.6 (2)		171.5 (4)	
H(2)···O(2)		1.706 (2)		1.711 (2)		1.721 (4)	
O(1)—H(2)···O(2)		174.5 (2)		174.7 (3)		174.7 (4)	

Temperature effect on the structure

In addition to refining the lattice parameters at the three data-collection temperatures, their changes were monitored during cooling and heating, see Fig. 2. Despite the higher standard deviations of the latter values due to the lower temperature stability at the intermediate points, a consistent trend can be established. Unlike the normal cases, where a shrinking of the unit cell is almost always observed, the (*a*,*b*) axes increase by 0.25 (1)% on cooling, while the length of the *c* axis increases only slightly by 0.10 (1)%. Nevertheless, no indications of a possible phase transition (change of space-group symmetry) could be detected. Due to the non-linear changes of the lattice constants, thermal expansion coefficients were not derived.

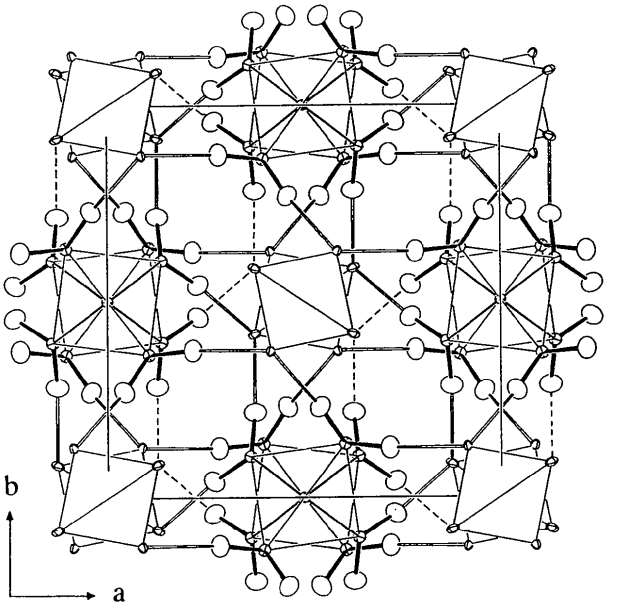

Fig. 1. Structure of $BeSO_4.4H_2O$ seen along [00$\bar{1}$] with arbitrary atomic radii (Johnson, 1976). The sulfate ions are drawn as open tetrahedra with S atoms omitted. Hydrogen bonds are represented by open lines, those to symmetry-related sulfate O atoms (not drawn) are dashed.

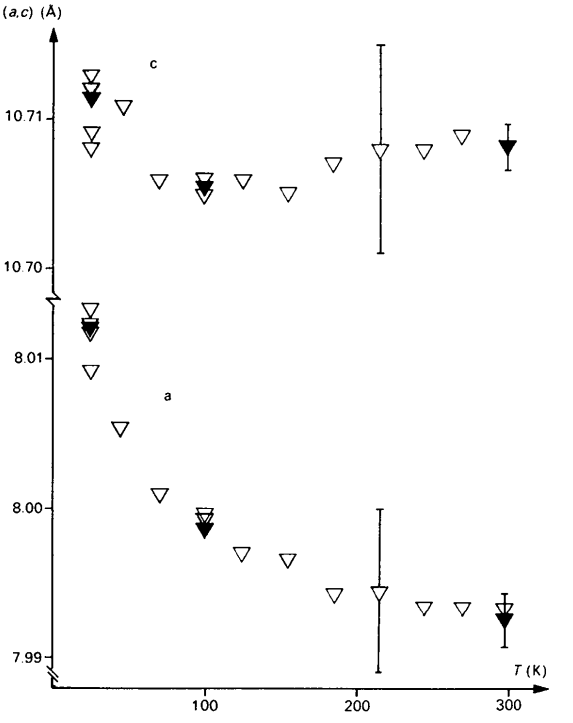

Fig. 2. Temperature dependence of the lattice parameters. Filled symbols represent values at data-collection temperatures. Representative e.s.d.'s for the open and filled-in symbols, respectively, are indicated as error bars.

The Be—O distance of 1.614 (1) Å in the $[Be(H_2O)_4]^{2+}$ cation is close to the mean value for the few other beryllium salt hydrates which have been structurally characterized, *e.g.* 1.616 Å in $Be(NO_3)_2.4H_2O$ (room-temperature X-ray data; Divjakovic, Edenharter, Nowacki & Ribár, 1976) or 1.617 Å in $Be[C_2(COO)_2].4H_2O$ (15 K neutron data; Robl, Hentschel & McIntyre, 1992). For the latter compound, an enlargement of the HOH angle (mean value 112.7°) similar to the present case (111.4°) was reported. This is a significant increase relative to the gas-phase value for free H_2O (104.5°; Benedict, Gailer & Plyler, 1956) and also relative to the mean value for solid hydrates of class 1 (107°; Chiari & Ferraris, 1982), see further below.

Deformation electron densities

Dynamic multipole model deformation maps for sections of interest around the water molecule and the hydrogen bonds are shown in Figs. 3 and 4. In all figures, the atoms defining the planes displayed are without parentheses, other atoms close to these sections are indicated in parentheses. In order to evaluate the characteristic features of the Be^{2+} ion and the water molecules separately, partial maps are plotted which include only the deformation functions of the Be^{2+} ion, the water molecule or the SO_4^{2-} ion, respectively.

(*a*) *Static versus dynamic maps.* 'Static' maps with the displacement parameters of all atoms set to zero, calculated to assess the influence of thermal motion on the electron deformation density, revealed only slight differences. The maximum and minimum peak heights increased by 0.05 e $Å^{-3}$ at most. This common procedure of obtaining 'static' maps simply enhances the features already present in the dynamic maps, whereas details lost due to 'thermal smearing' cannot be recovered. Such effects are slightly noticeable in the 30 K maps, but are significantly more pronounced in the 100 K maps (now shown). This emphasizes that where the highest achievable accuracy for the electron density is desired, the data-collection temperature should be as low as possible. Although arguments along these lines have been presented by other authors (see, for instance, Destro & Marsh, 1984), the consequences have probably been underestimated.

(*b*) *Electrostatic and polarization contributions.* Hydrogen bonding can schematically be decomposed into electrostatic, polarization, charge-transfer, exchange and dispersion contributions (*e.g.* Morokuma, 1971). A similar approach applies to the coordination of metal ions. The electrostatic component is largely dominant on the energy scale and corresponds to a reorientation of the molecules in question. That leads in the present case to the trigonal coordination geometry around the water O atoms. The remaining factors can hardly be observed separately in an experimental electron-density study, but it is well known from quantum chemical calculations that the polarization contribution (*i.e.* the deformation of the charge distribution of the free molecules/ions without any charge transfer) has the largest effect within this group. We can assess the extent of polarization from the deformation density maps, but it is difficult to derive reliable individual

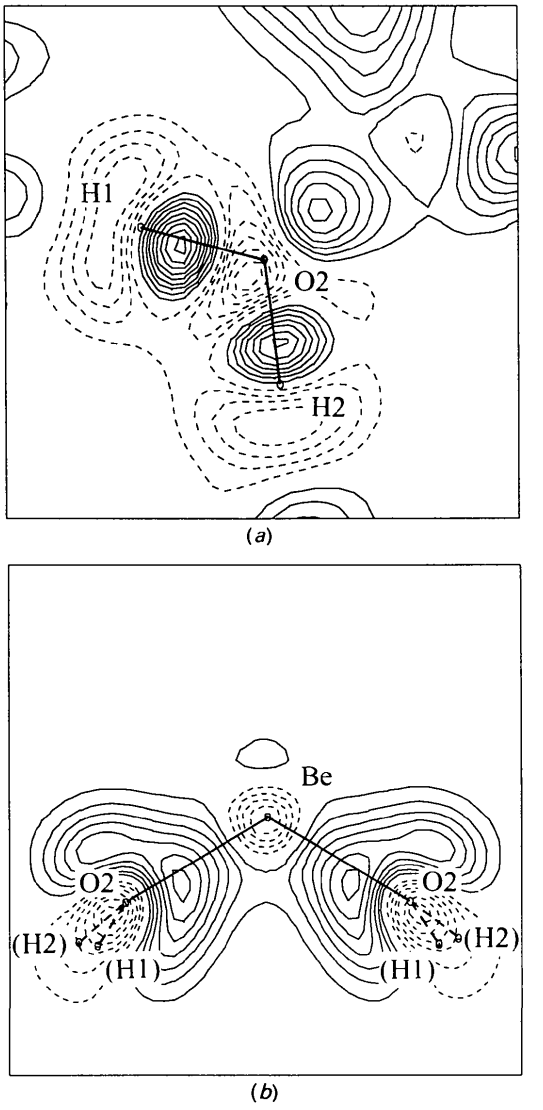

Fig. 3. The deformation electron density of the water molecule in $BeSO_4.4H_2O$ plotted in various sections of interest: (*a*) H—O—H plane; (*b*) O—Be—O plane. The maps include the deformation functions of all atoms. Bonds to atoms deviating from the depicted planes are drawn as dashed lines, such atoms are labelled in parentheses. Static maps, contour intervals at 0.05 e $Å^{-3}$, positive contours are represented by full lines, negative contours dashed, zero level omitted.

atomic charges, since that procedure is very sensitive to the partitioning scheme. However, this is not crucial for a discussion of the polarization *per se*.

Although no symmetry constraints were imposed on the water O atom, the water deformation density approaches *mm*2 (C_{2v}) symmetry, which reflects the (pseudo-) symmetry of the nearest-neighbour environment. This also indicates that the maps obtained are chemically reasonable. The map of the O—Be—O plane, which is essentially normal to the H—O—H plane, shows a pronounced distortion of the oxygen lone-pair density towards the Be^{2+} ion. There is only one maximum in the oxygen lone-pair region with a peak height of 0.55 e $Å^{-3}$. The polarizing influence of the beryllium ion is, therefore, strong.

These experimental results compare well with *ab initio* calculations on a $Be^{2+}\cdots OH_2$ complex (Hermansson, Olovsson & Lunell, 1984), see Fig. 5. The geometry of this model complex has actually been taken from the $BeSO_4.4H_2O$ structure data given by Sikka & Chidambaram (1969). Although the calculations do not take the influence of the hydrogen bond acceptors into account, charge accumulation on the Be···O bond axis in the oxygen lone-pair region and an additional charge depletion

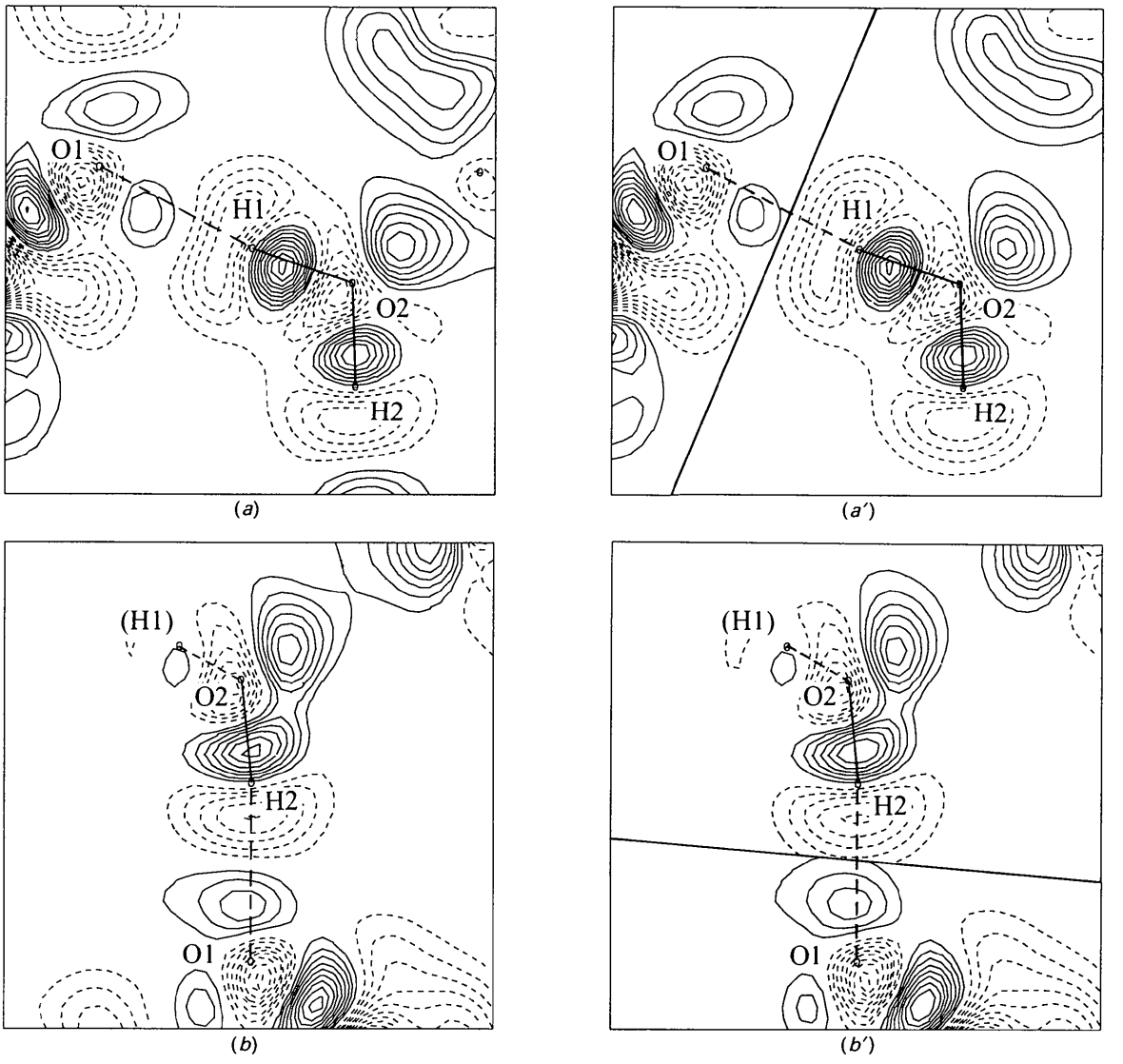

Fig. 4. The deformation electron density of the hydrogen bonds in $BeSO_4.4H_2O$: (*a*) for the plane O—H(1)···O(1), which is very close to the HOH plane; (*b*) for the plane O(2)—H(2)···O(1). The primed maps are constructed from the individual maps of the water molecule and the sulfate ion, the heavy lines indicate the limits of the respective regions. Hydrogen bonds are represented as long dashed lines. See Fig. 3 for more explanations.

close to the H atoms is calculated (compared with the free water molecule as a reference state). This is in complete qualitative agreement with the experiment.

It has been shown that a change in the intramolecular geometry of a water molecule (without any other external forces) is accompanied by a change in the electron redistribution, but this effect is small compared with the changes which arise from the coordination to a cation (Hermansson, Olovsson & Lunell, 1984; Hermansson, 1985). We conclude, therefore, that the cation–oxygen interaction has the dominant effect on the distortion of the electron density in the oxygen lone-pair region. A (subsequent) change in the HOH angle is relatively easy to accomplish if other factors, such as the arrangement of the hydrogen-bond acceptors, do not interfere strongly. This explains both the enlargement of the (average) HOH angle for trigonally coordinated water molecules and the relatively large scatter found for different compounds, even when the water molecules are grouped into classes according to their coordination geometry (see Chiari & Ferraris, 1982). It is not too surprising that there are cases where a significant increase in the HOH angle for trigonally coordinated water molecules is not observed (*e.g.* by Robl & Kuhs, 1991). Sometimes, the reported HOH angles are likely to be too large because of an inappropriate treatment of thermal motion effects, which are especially prominent for trigonally coordinated water molecules (see the discussion given by Kellersohn, Lutz, Vogt, Delaplane & Olovsson, 1992). Such effects do not influence the present results, however.

(*c*) *The synergetic effect of the beryllium ion.* The polarizing effect of the Be^{2+} ion is transferred *via* the O—H bonds to the hydrogen bonds: the electron deficiency close to H amounts up to -0.20 e Å^{-3} in both cases, which is deeper than in tetragonal $NiSO_4.6H_2O$ as well as in monoclinic $CoSO_4.6H_2O$, where the corresponding deficiencies were on average between -0.10 and -0.15 e Å^{-3}. The hydrogen bonds in $BeSO_4.4H_2O$ are on average about 0.15 Å shorter than those for these two compounds.

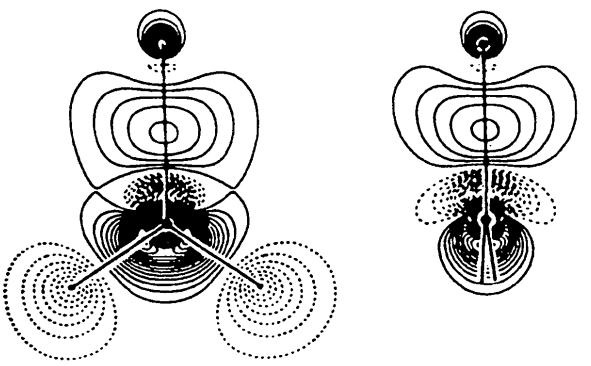

Fig. 5. The calculated changes in the electron distribution of a water molecule upon interaction with a Be^{2+} ion at a distance of 1.62 Å; DZP basis; $\Delta\rho = \rho(\text{total}) - [\rho(\text{free } H_2O) + \rho(Be^{2+})]$, contour lines at 0.02 e Å^{-3}; taken from Hermansson, Olovsson & Lunell (1984).

This reflects the increased hydrogen-bond strength in the title compound. An increase of hydrogen-bond strength with increasing metal–oxygen interactions has already been established from vibrational spectroscopic studies as well as theoretical calculations. It has been called the 'synergetic effect' (Lutz, 1988) and the present study reveals, perhaps for the clearest case so far, that this synergetic effect is also evident from the electron-density distribution. The decoupled OH stretching frequencies are observed at 2908 and 3140 cm^{-1} for OH(1) and OH(2), respectively (100 K, IR data, Pigenet 1982*a*); their mean downshift relative to the free HDO molecule is 683 cm^{-1} (for the free HDO molecule, ν_{OH} = 3707 cm^{-1}; Benedict, Gailor & Plyler, 1956).

The OH stretching frequencies differ by 145 cm^{-1}, but no significant difference is found for the two different hydrogen bonds in the electron deficiency region beyond the H atom. However, the electron excess in the OH bond is somewhat larger for H(1) than for H(2), but it is probably beyond the accuracy of our data to allow a discussion of these small differences.

(*d*) *The influence of the* γ *parameter on the partial maps.* A partitioning of the deformation density shows severe superposition effects between Be^{2+} and the water O atom when the 'conventional' γ value of 3.5 is used, *i.e.* the Be functions extend far into the oxygen lone-pair region. Since γ governs the radial decay of these functions, a higher γ value contracts the deformation functions closer to the nucleus. This is illustrated in Fig. 6: for $\gamma = 3.5$ on all atoms, the individual maps display unrealistic features. However, when $\gamma = 5.0$ for Be and 3.5 for O are used, the individual maps become much more sensible, see Figs. 6(*a*) and 6(*b*). The *total* maps are almost insensitive to this modification, just like the refinement indicators as *R* values and goodness-of-fit. We should just note the higher electron deficiency close to the oxygen core in the former case. It is not surprising that the partitioning procedure with the more delocalized deformation functions succeeded comparably well for $NiSO_4.6H_2O$, since the metal–oxygen interaction is much weaker in the latter case.

In contrast, the hydrogen-bond regions show less severe superposition, although the hydrogen bonds are strong. This again demonstrates that the electrostatic interaction is the main contribution when hydrogen bonds are formed. Nevertheless, the competition between the enhancement of the features due to polarization by hydrogen bonding (and the far-

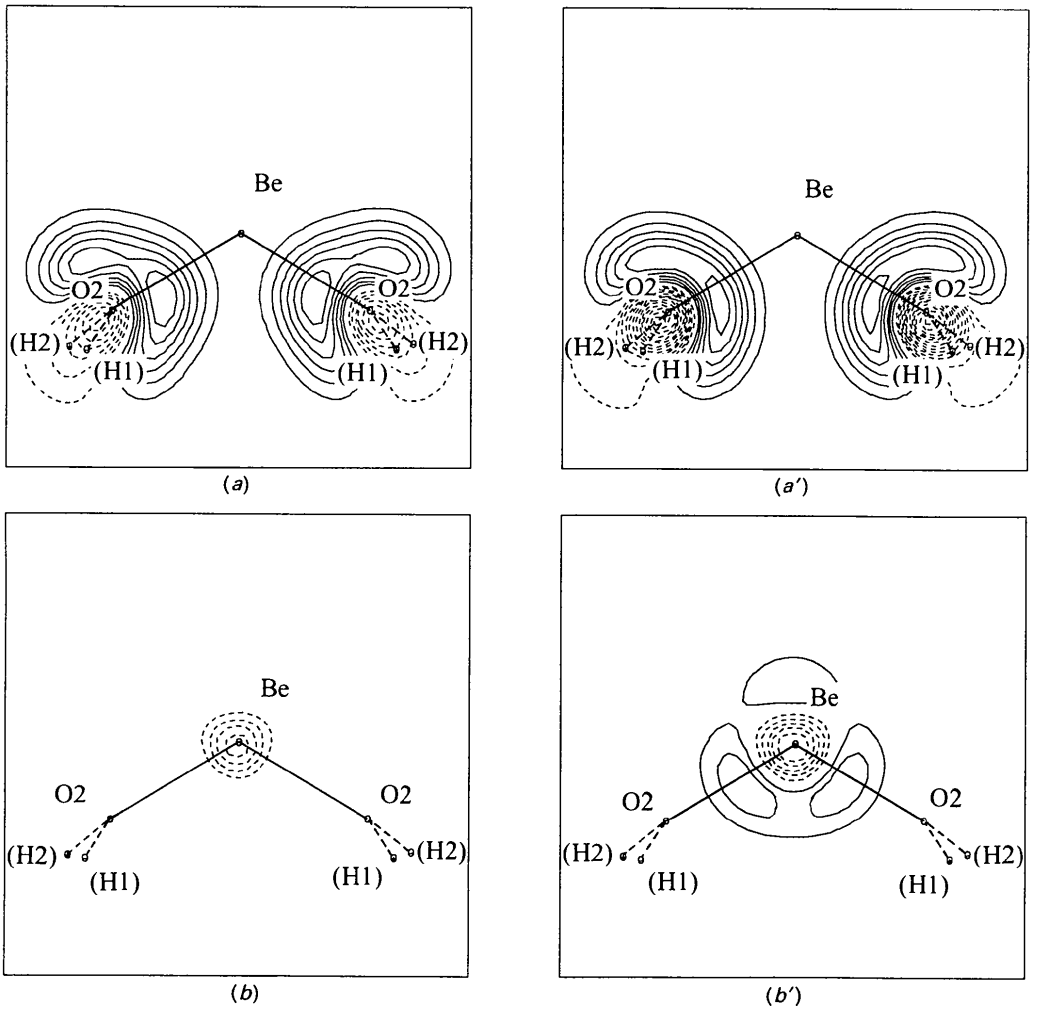

Fig. 6. The influence of the γ parameter on the individual deformation densities: (*a*) only H_2O functions, (*b*) only Be functions. The unprimed maps are calculated with the γ parameters given in the text, the primed maps are for $\gamma = 3.5$ for all atoms. To be compared with Fig. 3(*b*) where the same section is displayed, see Fig. 3 for more explanations.

reaching polarization transfer caused by the Be coordination) and their reduction due to superposition effects can clearly be recognized by comparing the total and the individual maps, see Figs. 4(*b*) and 4(*b'*). For a general discussion of the superposition effect, see Olovsson, Ptasiewicz-Bak & McIntyre (1993).

We would like to thank Mr H. Karlsson and Mr H. Rundlöf for their skillful technical assistance with the data collections. Financial support has been provided by the Deutsche Forschungsgemeinschaft and the Swedish Natural Science Research Council, which is gratefully acknowledged.

References

Abrahams, S. C. & Keve, E. T. (1971). *Acta Cryst.* A**27**, 157–165.
Becker, P. & Coppens, P. (1974*a*). *Acta Cryst.* A**30**, 129–147.
Becker, P. & Coppens, P. (1974*b*). *Acta Cryst.* A**30**, 148–153.
Becker, P. & Coppens, P. (1975). *Acta Cryst.* A**31**, 417–425.
Beevers, C. A. & Lipson, H. A. (1932). *Z. Kristallogr.* **82**, 297–308.
Benedict, W. S., Gailer, N. & Plyler, E. K. (1956). *J. Chem. Phys.* **24**, 1139–1165.
Berglund, B. & Tegenfeldt, J. (1977). *J. Mol. Struct.* **39**, 207–217.
Chiari, G. & Ferraris, G. (1982). *Acta Cryst.* B**38**, 2331–2341.
Dance, I. G. & Freeman, H. C. (1969). *Acta Cryst.* B**25**, 304–310.
Destro, R. & Marsh, R. E. (1984). *J. Am. Chem. Soc.* **106**, 7269–7271.
Divjakovic, V., Edenharter, A., Nowacki, W. & Ribár, B. (1976). *Z. Kristallogr.* **144**, 314–322.
Harel, M. & Hirshfeld, F. L. (1975). *Chem. Scr.* **26**, 389–394.
Hermansson, K. (1985). *Acta Cryst.* B**41**, 161–169.
Hermansson, K., Olovsson, I. & Lunell, S. (1984). *Theor. Chim. Acta*, **64**, 265–276.
Hirshfeld, F. L. (1971). *Acta Cryst.* B**27**, 769–781.
Hirshfeld, F. L. (1977). *Isr. J. Chem.* **32**, 226–229.

JOHNSON, C. K. (1976). *ORTEPII*. Report ORNL 5138, Oak Ridge National Laboratory, Tennessee, USA.
KATIYAR, R. S. & KRISHNAMURTHY, N. (1969). *Ind. J. Pure Appl. Chem.* **7**, 95–97.
KELLERSOHN, TH., DELAPLANE, R. G. & OLOVSSON, I. (1991). *Sagamore X, Collected Abstracts*, pp. 62–63. Germany: Konstanz.
KELLERSOHN, TH., DELAPLANE, R. G., OLOVSSON, I. & MCINTYRE, G. J. (1993). *Acta Cryst.* B**49**, 179–192.
KELLERSOHN, TH., LUTZ, H.D., VOGT, TH., DELAPLANE, R. G. & OLOVSSON, I. (1992). *Acta Cryst.* B**48**, 166–172.
LARSSON, K. & TEGENFELDT, J. (1988). *J. Mol. Struct.* **176**, 303–312.
LARSSON, K., TEGENFELDT, J. & HERMANSSON, K. (1991). *J. Chem. Soc. Faraday Trans.* **87**, 1193–1200.
LEHMANN, M. S. & LARSEN, F. K. (1974). *Acta Cryst.* A**30**, 580–584.
LUNDGREN, J. O. (1982). *Crystallographic Computer Programs*, Report UUIC-B13-04-05. Institute of Chemistry, Univ. of Upsala, Sweden.
LUTZ, H. D. (1988). *Struct. Bonding Berlin*, **69**, 97–125.
MCINTYRE, G. J., PTASIEWICZ-BAK, H. & OLOVSSON, I. (1990). *Acta Cryst.* B**46**, 27–39.
MOROKUMA, K. (1971). *J. Chem. Phys.* **55**, 1236–1244.
OLOVSSON, I., PTASIEWICZ-BAK, H. & MCINTYRE, G. J. (1993). *Z. Naturforsch. Teil A*, **48**, 3–11.
PIGENET, C. (1982*a*). *J. Raman Spectr.* **13**, 66–77.
PIGENET, C. (1982*b*). *J. Raman Spectr.* **13**, 262–269.
ROBL, C., HENTSCHEL, ST. & MCINTYRE, G. J. (1992). *J. Solid State Chem.* **96**, 318–323.
ROBL, C. & KUHS, W. F. (1991). *J. Solid State Chem.* **92**, 101–109.
SAMSON, S., GOLDISH, E. & DICK, C. F. (1980). *J. Appl. Cryst.* **13**, 425–432.
SEARS, V. F. (1986). In *Neutron Scattering, Methods of Experimental Physics*, Vol. 23, edited by K. SKÖLD & D. L. PRICE, pp. 521–550. New York: Academic Press.
SIKKA, S. K. & CHIDAMBARAM, R. (1969). *Acta Cryst.* B**25**, 310–315.
SOULMAGNON, R. & COUTURE-MATHIEU, L. (1950). *C. R. Acad. Sci.* **231**, 129–131.
SRIVASTAVA, B. K., KHANDELWAL, D. P. & BIST, H. D. (1976*a*). *Pramana*, **7**, 49–55.
SRIVASTAVA, B. K., KHANDELWAL, D. P. & BIST, H. D. (1976*b*). *Pramana*, **7**, 401–406.
THORNLEY, F. R. & NELMES, R. J. (1974). *Acta Cryst.* A**30**, 748–757.
UNGER, B. (1972). *Phys. Status Solidi B*, **49**, 107–116.

Acta Cryst. (1994). B**50**, 326–332

Distortion in the $CdS_{1-y}Se_y$ Lattices: an Example of Relaxation in Wurtzite Compounds

BY ALAIN MARBEUF

Laboratoire de Cristallographie et Physique Cristalline associé au CNRS, Université Bordeaux I, 351 *Cours de la Libération, F*33405 *Talence CEDEX, France*

MICHEL BARBE

Laboratoire de Physique des Solides de Bellevue, CNRS, 1 *Place A.-Briand, F*92195 *Meudon CEDEX, France*

ALINE RAMOS

Laboratoire de Minéralogie et Cristallographie associé au CNRS, Universités Paris VI *et Paris* VII, 4 *Place Jussieu, F*75252 *Paris CEDEX* 05, *France*

CLAIRE LEVELUT

Laboratoire de Sciences des Matériaux Vitreux associé au CNRS, Université de Montpellier II, *Place Eugène Bataillon, F*34095 *Montpellier CEDEX, France*

AND SOPHIE WSZOLEK

Laboratoire de Physique des Solides de Bellevue, CNRS, 1 *Place A.-Briand, F*92195 *Meudon CEDEX, France*

(*Received* 19 *July* 1993; *accepted* 2 *December* 1993)

Abstract

Relaxation in pseudobinary wurtzite lattices is predicted using the valence force field (VFF) approach. In this hexagonal packing structure, the computer simulation of the quasi-tetrahedral alloy lattice at an arbitrary composition is carried out by searching atomic positions at which the elastic forces acting